Article

Effect of Build Parameters on the Compressive Behavior of Additive Manufactured CoCrMo Lattice Parts Based on Experimental Design

Orhan Gülcan [1,*], Ugur Simsek [1], Okan Cokgunlu [2], Mirhan Özdemir [2], Polat Şendur [2] and Guney Guven Yapici [2]

1 General Electric Aviation, Additive Design, Kocaeli 41400, Turkey; ugur.simsek@ge.com
2 Mechanical Engineering Department, Ozyegin University, Istanbul 34794, Turkey; okan.cokgunlu@ozu.edu.tr (O.C.); mirhan.ozdemir@ozu.edu.tr (M.Ö.); polat.sendur@ozyegin.edu.tr (P.Ş.); guven.yapici@ozyegin.edu.tr (G.G.Y.)
* Correspondence: orhan.gulcan@ge.com; Tel.: +90-262-677-8410

Abstract: Due to their high specific strength, toughness, and corrosion and wear resistance characteristics, CoCrMo alloys are widely used in different industries and applications: wind turbines and jet-engine components, orthopedic implants, dental crowns, etc. The aim of this paper is to investigate the effect of lattice parameters on the compressive behavior of laser powder bed fusion (LPBF) parts from CoCrMo material. Build orientation, volume fraction, and lattice type are chosen as input parameters or control factors, and compressive yield strength (σ_y), elastic modulus (E), and specific energy absorption are chosen as the output or performance parameters for optimization. The Taguchi experimental design method is used in the arrangement of lattice parameters during experimental studies. The level of importance of the lattice parameters on σ_y, E, and specific energy absorption is determined by using analysis of variance (ANOVA). At the same material volume fractions, Diamond specimens showed higher σ_y and specific energy absorption than Gyroid and Primitive specimens, except σ_y at 0.4 volume fraction, where a Gyroid specimen showed the best result. The experimental and statistical results revealed that volume fraction and build orientation were found to be the major and minor effective factors, respectively, for all performance parameters (σ_y, E, and specific energy absorption). The effect of volume fraction on σ_y, E, and specific energy absorption was found to be 85.11%, 91.83%, and 57.71%, respectively. Lattice type was found to be the second-ranking factor, affecting σ_y, E, and specific energy absorption with contributions of 11.04%, 6.98%, and 39.40%, respectively. Multi objective optimization based on grey relation analysis showed that a Diamond specimen with 0.4 volume fraction and 45° build orientation was the best parameter set for the investigated performance outputs.

Keywords: additive manufacturing; laser powder bed fusion; build orientation; volume fraction; lattice type

1. Introduction

The necessity of using light and durable materials in aviation, automotive, sports, and biomedical industries has led researchers to investigate different types of materials and structures in several applications. Lattice structures are one type of such structures that have received great attention in recent years. These are three-dimensional structures consisting of one or more repeating unit cells [1]. Compared to solid monolithic structures, these structures have been used in different applications due to their ability to absorb higher energy, to provide higher sound insulation, and their thermal management capability [2,3]. Lattice structures can be categorized as strut-based lattice structures, shell lattice structures, and triply periodic minimum surface (TPMS) lattice structures in terms of their geometrical shapes [4].

TPMS lattice structures are three-dimensional structures formed by mathematical equations, and have zero mean curvature. They were first investigated by Schwarz in 1856. He expressed the surfaces created as Diamond and Primitive. Neovius further advanced the study and obtained a Primitive cubic (C(P)) surface [5]. In the 1960s, Schoen proposed IWP (I-Graph-Wrapped Package), FRD (F-Rhombic Dodecahedron), and G (Gyroid) surfaces [6]. Fischer and Koch in 1987 [7] and Gozdz and Holyst in 1990 [8] discovered new TPMS surfaces after their long studies.

Complex geometries of TPMS structures make the manufacturing of these structures very difficult, but today, additive manufacturing (AM) provides novel solutions for the production of different types of TPMS structures. Laser Powder Bed Fusion (LPBF) is one of the metal AM processes where metal powders are placed on a build plate with an amount of pre-defined thickness by recoater blade, and a laser source is used to selectively melt the powder according to computer-aided design geometry in an inert gas atmosphere. When one layer is scanned and melted, the build plate is lowered with an amount of layer thickness, and the new layer of powder is laid on the previous layer. This process continues until the final part is fully formed [9].

In scientific literature, a number of studies have focused on the mechanical properties of different types of TPMS lattice structures produced by AM. In terms of their mechanical behaviors, TPMS structures can show stretch-dominated or bending-dominated behaviors [10]. It was reported that Primitive structures have higher elastic modulus (E) and compressive strength, and show stretch-dominated behavior than Diamond and Gyroid structures, which have bending-dominated behaviors, based on the experimental results with selective laser-sintered specimens from PA 2200 material. Therefore, it was suggested to use Primitive structures in applications where high strength is needed, and Diamond and Gyroid structures in applications where high strain before plastic deformation is needed [11]. In another study, Restrepo et al. [12] compared ceramic Primitive-, Gyroid-, and Diamond-type lattice structures, and concluded that Primitive showed the highest E and yield strength (σ_y), whereas Gyroid showed the lowest values. Castro et al. [13] compared the compressive behavior of Diamond, Primitive, and Gyroid TPMS structures from Visijet M3 Crystal material with different volume fractions (0.2, 0.3, and 0.4). Their study revealed that a Diamond structure with 0.4 volume fraction showed the highest elastic modulus and yield stress. On the other hand, a Diamond structure with 0.2 volume fraction showed the lowest elastic modulus, and a Primitive structure with 0.2 volume fraction showed the lowest yield stress. Abueidda et al. [14] compared the mechanical properties of selective laser-sintered Gyroid structures with Neovius, IWP, and Primitive structures from PA 2200 material. They stated that Neovius and IWP structures showed the highest and a Primitive structure showed the lowest compressive strength and energy absorption ability. Al Mahri et al. [15] studied the quasi-static and dynamic response of Gyroid, Diamond, IWP, Primitive, and Fisher Kock TPMS lattice structures produced with an LPBF process from 316L stainless steel. Their results revealed that IWP showed the highest and Primitive showed the lowest plateau stress in both loading conditions. In terms of energy absorption ability, Diamond offers the highest and Primitive offers the lowest values. Zhang et al. [16] stated that a Diamond structure showed higher mechanical properties than Gyroid and Primitive structures produced with LPBF from 316L stainless steel material. Liang et al.'s study [17] on 316L stainless steel LPBF-manufactured Gyroid and Primitive structures showed that the Primitive structure showed stretch-dominated behavior, and the Gyroid structure showed bending-dominated behavior. Moreover, the Primitive structure showed higher energy absorption ability than the Gyroid structure at low relative densities. Novak et al. [18] compared quasi static and dynamic compressive behavior of LPBF-produced 316L stainless steel Diamond, Gyroid, IWP, and Primitive TPMS structures, and stated that the Diamond structure showed the highest and the Primitive structure showed the lowest plateau stress and specific energy absorption. Shi et al. [19] investigated compressive and energy absorption behavior of LPBF-produced Ti6Al4V Gyroid, Primitive, Diamond, and IWP TPMS structures, and stated that the Gyroid and IWP

structures showed higher plateau stress and energy absorption than other TPMS structures. They also stated that for Gyroid and IWP structures, elastic modulus and yield stress increased with increasing relative density. It is clear from this short literature survey that the mechanical properties of different types of AM-produced TPMS lattice structures in the literature might be contradictory due to the manufacturing methods, defects, dimensional variations, and surface roughness of manufactured specimens [4].

Apart from the type, the mechanical properties of TPMS lattice structures are affected by build orientation and volume fraction [20]. Cai et al. [21] investigated the effect of porosity on mechanical properties of PLA Diamond TPMS structures. They stated that low-porosity samples had 3 times higher yield stress and 2.5 times higher elastic modulus than high-porosity samples. The build orientation effect on mechanical properties was studied by Alsalla et al. [22] for LPBF-manufactured 316L Gyroid lattice structures. They stated that vertically-oriented samples showed 60% higher σ_y than horizontally-oriented ones. The main reason for the effect of different build orientations on the mechanical properties is the different porosity values for build parts. Delroisse et al. [23] stated that LPBF-manufactured AlSi10Mg vertically-built samples showed a lower amount of porosity than samples with different build angles. It is also worth noting that build orientation affects the microstructural development in LPBF-printed specimens. In LPBF, usually, columnar grains oriented in the build direction are formed [24], and these grains are long and thin at the bottom of the specimens near the build plate due to large thermal gradients and high cooling rates [25] and become coarser at higher build heights due to the lower thermal gradients between successive layers [26]. However, the microstructure development in lattice structures is more complicated and diverse [27], which affects the mechanical properties of the printed specimen [28].

As can be seen from the aforementioned literature, there has been many studies performed about investigating the effect of build orientation, volume fraction, and different types of lattice structures on mechanical performance, especially on E and σ_y. It is also very important to know the significance of the effect of these parameters on mechanical properties so that the design engineer can have the knowledge to change the parameters in the right order to acquire the intended strength and improve the quality of AM parts. However, most of the research works focused on the effect of process parameters on mechanical properties. For instance, in one of the studies, laser power, scan speed, hatch spacing, and layer thickness were chosen as design parameters, and correlations between these parameters were shown in LPBF-produced Inconel 718 specimens [29]. In another study, Dong et al. [30] used Taguchi analysis to find the optimum process parameters for the mechanical properties of fused deposition modelled ABS lattice parts. They used nozzle temperature, print speed, fan speed, and layer height as input parameters to be optimized for two different type of lattice structure: horizontal and inclined struts. To the best of the authors' knowledge, there are limited studies on the percent contribution of geometrical parameters (build orientation, volume fraction, and lattice type) on the mechanical properties of TPMS lattice-structured metal parts produced by LPBF. Moreover, most of the research works related with LPBF processes used Ti6Al4V, 316L stainless steel, AlSi10Mg, and nickel-based superalloys such as Inconel 718. Moreover, it was observed that no studies have focused on the mechanical properties of Gyroid, Diamond, and Primitive lattice structures produced by LPBF from CoCrMo material so far. In their study, Park et al. [31] used CoCrMo powder material to produce IWP and Neovius TPMS structures with the LPBF method and compared the mechanical properties of these lattices under compression.

To fill these gaps, this experimental research focuses on the impact of three different parameters (build orientation, volume fraction, and lattice type) on *E*, σ_y, and the specific energy absorption of lattice structures produced by LPBF using CoCrMo alloy. The Taguchi experimental design method is used in the settings of lattice parameters during experimental studies. The level of importance of the lattice parameters on *E*, σ_y, and specific energy absorption is determined by using analysis of variance (ANOVA) analysis.

2. Materials and Methods

2.1. Design of Experiment Based on Taguchi Method

One of the disadvantages of classical experimental design methods is their complexity and difficulty. Additionally, when the number of input parameters increases, large number of experiments have to be carried out. Moreover, the LPBF method currently has a high cost; therefore, rather than performing a full factorial design of experiment, reducing the quantity of specimens and cost is essential by using other experimental methods. For these reasons, in this study, the L_9 orthogonal array based on the Taguchi method was used to optimize σ_y, E, and specific energy absorption values. According to the Taguchi method, the L_9 orthogonal array table consists of three control parameters and three levels as shown in Table 1. The combination of these parameters and levels for each specimen are shown in Table 2.

Table 1. Lattice parameters used in the experiments.

Lattice Parameters	Symbol	Level 1	Level 2	Level 3
Volume fraction	A	0.2	0.3	0.4
Build orientation (°)	B	45	60	90
Lattice type	C	Gyroid	Diamond	Primitive

Table 2. Experimental design using L9 orthogonal array.

Specimen No	A	B	C
1	1	1	1
2	1	2	2
3	1	3	3
4	2	1	2
5	2	2	3
6	2	3	1
7	3	1	3
8	3	2	1
9	3	3	2

Process parameters (laser power, laser spot size, hatch spacing, layer thickness, etc.) also affect the mechanical behavior of LPBF-produced parts. However, in this study, only geometrical parameters were considered. There are different geometrical parameters that can be used as design variables, but volume fraction, build orientation, and lattice types were chosen in this study, since they are the basic parameters that need to be taken into account in lattice design studies. Gyroid, Diamond, and Primitive lattice types are widely used in different applications. Therefore, these three lattice types were chosen in the study. It is well known that 45° with respect to build plate is the threshold value under which any overhang surfaces need to be supported in the LPBF process. Therefore, 45, 60, and 90° build orientations were chosen as design variables. Lastly, preliminary studies showed that 0.5 and larger volume fraction values resulted in nearly bulk, solid pieces. Therefore, three different volume fraction values less than 0.5 were used in the study.

In each experiment, three performance characteristics, namely, σ_y, E, and specific energy absorption were investigated. In the Taguchi method, a loss function is used to calculate the deviation between the experimental value and the desired value. This loss function is further transformed into a signal-to-noise (S/N) ratio. There are several S/N ratios available depending on the type of characteristics; lower is better (LB), nominal is best (NB), and higher is better (HB). Since higher σ_y, E, and specific energy absorption means higher performance, HB is selected for obtaining optimum lattice parameter characteristics. The S/N ratio for HB can be calculated by using Equation (1).

$$\eta = -10 \log \left[\frac{1}{n} \sum_{i=1}^{n} \frac{1}{y_i^2} \right] \tag{1}$$

where η denotes the S/N ratio calculated from the observed values (unit: dB), y_i represents the experimentally observed value of the ith experiment, and n is the repeated number of each experiment [32].

The S/N ratios determined from the experimental observed values were statistically studied by ANOVA to explore the effects of each input parameter on the observed values and to elucidate which building parameters significantly affected the observed values.

2.2. Specimen Design and Manufacturing

Primitive, Diamond, and Gyroid structures are three types of TPMS structures modelled with the mathematical formulas below:

$$Primitive: cosx + cosy + cosz = c \tag{2}$$

$$Gyroid: sinx \times cosy + siny \times cosz + sinz \times cosx = c \tag{3}$$

$$Diamond: cosx \times cosy \times cosz - sinx \times siny \times sinz = c \tag{4}$$

In these expressions, $x = 2\pi X/L_x$; $y = 2\pi Y/L_y$; $z = 2\pi Z/L_z$; L_x, L_y, and L_z are unit cell dimensions; c is a constant; and X, Y, and Z are the number of unit cells in the x, y, and z directions, respectively [33]. In this study, 8 mm unit cell dimensions and 4-unit cells in each direction were used. Therefore, specimens with 32 mm × 32 mm × 32 mm dimensions were modelled and manufactured.

Primitive, Diamond, and Gyroid structures were modelled using Siemens NX 12 software (Siemens AG, Munich, Germany). The specimens were located on the build plate, as shown in Figure 1, where the powder recoater direction is from right to left. For each configuration of 3 factors, three specimens, in other words, repetitions, and a total of 27 specimens were produced in two builds.
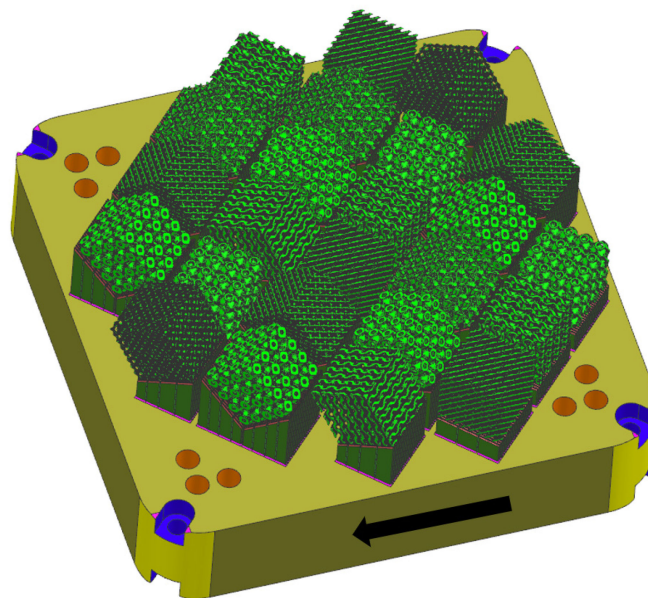

Figure 1. Build layout. Black arrow shows powder recoater direction.

After 3D CAD model preparation, the build layout was converted into stl format to be used in the LPBF machine. The specimens were manufactured using a Concept Laser M2 LPBF machine (Concept Laser GmbH, Lichtenfels, Germany) with 50 μm layer thickness, 180 W laser power, 1500 mm/s scanning speed, and 60 μm hatch spacing under an Argon gas environment. Gas atomized spherical CoCrMo powder material with 10–45 μm particle size from GE Additive (GE Additive, Mölnlycke, Sweden) was used in the production. CoCrMo alloys have very high specific strength, toughness, corrosion, and wear resistance, and due to these characteristics, they are used in different industries,

ranging from aviation to biomedical industries. Wind turbine and jet engine components, dental and orthopedic implants, hip and knee joints, etc. are some of the applications in which CoCrMo material is used [34,35]. Due to these superior characteristics and wide application areas, CoCrMo powder material was used in the present study. The chemical composition of the powder is shown in Table 3.

Table 3. Chemical composition of CoCrMo powder.

Element	Co	Cr	Mo	C	Ni	Fe	Mn, Si	Others
wt%	Bal.	27.0–30.0	5.0–7.0	Max. 0.35	Max. 0.50	Max. 0.75	Max. 1.0	Max. 0.58

After manufacturing, a wire electrical discharge machine (Agie Charmilles Ltd., Biel, Switzerland) with a wire thickness of 0.3 mm and an average cutting speed of 5 mm/min was used for removing specimens from the build plate.

2.3. Test and Analysis

Quasi-static compression tests were performed on an Instron 5985 universal testing machine (Instron Inc., Norwood, MA, USA) with a fixed strain rate of 1×10^{-3} s^{-1}. Compression tests were performed up to 70% strain for all specimens. Load displacement curves were obtained after compression tests, and then, these curves were converted into stress-strain curves by taking 1024 mm^2 (32 mm $\times$ 32 mm) specimen area as cross-sectional area. Energy absorption (the area under load–displacement curve) was calculated by using Matlab software (2019b, MathWorks, Natick, MA, USA). After compression tests, specimen weights were measured with a Sartorius GC 1603 SOCE model weight measuring device. Specific energy absorption was then calculated by using energy absorption per unit mass. For ANOVA analysis, Minitab software (19.2020.1, Minitab Inc, State College, PA, USA) was used. Three tests were performed for each specimen, and average values of σ_y, E, mass, and energy absorption were used in the analysis.

3. Results and Discussions

All the specimens were manufactured without any specific production problem, as shown in Figure 2.
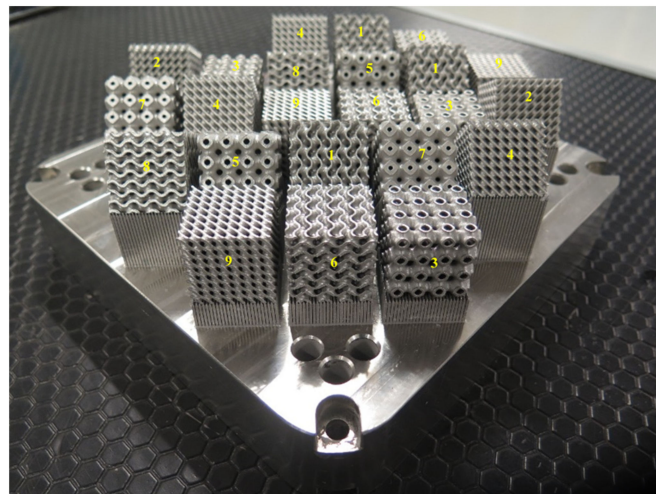

Figure 2. Manufactured specimens. Numbers on the figure represent the specimen no.

3.1. Quasi Static Compression Test Results

Average values of σ_y, E, and specific energy absorption for all specimens are shown in Table 4. Diamond specimens showed the highest and Primitive specimens showed the lowest σ_y and specific energy absorption, respectively. One exception is that for 0.4 volume fraction, the Gyroid specimens outperformed the Diamond specimens in terms of σ_y. For all

volume fractions, Gyroid specimens showed the highest and Primitive specimens showed the lowest *E*, respectively.

Table 4. σ_y, *E*, mass, and specific energy absorption values for all specimens.

Specimen No	σ_y (MPa)	E (GPa)	Specific Energy Absorption (J/g)
1	76.40 ± 1.10	2.34 ± 0.07	30.11 ± 0.91
2	103.35 ± 3.15	2.15 ± 0.04	37.74 ± 1.02
3	62.36 ± 1.86	1.79 ± 0.02	19.39 ± 0.64
4	158.24 ± 3.68	3.42 ± 0.13	51.36 ± 1.35
5	78.52 ± 2.12	3.02 ± 0.09	36.02 ± 0.88
6	136.46 ± 2.85	3.47 ± 0.04	42.14 ± 1.23
7	196.73 ± 2.25	4.10 ± 0.15	39.41 ± 1.15
8	236.34 ± 3.60	5.20 ± 0.22	47.47 ± 1.02
9	218.10 ± 3.54	4.70 ± 0.12	49.66 ± 1.42

Stress–strain graphs for all specimens under compressive loading are shown in Figures 3–5. It is well known that lattice structures generally go through three stages under compressive loads: elastic, plastic, and densification. In the elastic stage, the behavior of the lattice structure is elastic. When the yield limit is exceeded, the material deforms plastically. It was shown in different studies that the stress required for plastic deformation of bending-dominated structures is constant, whereas it oscillates for stretch-dominated structures [4].
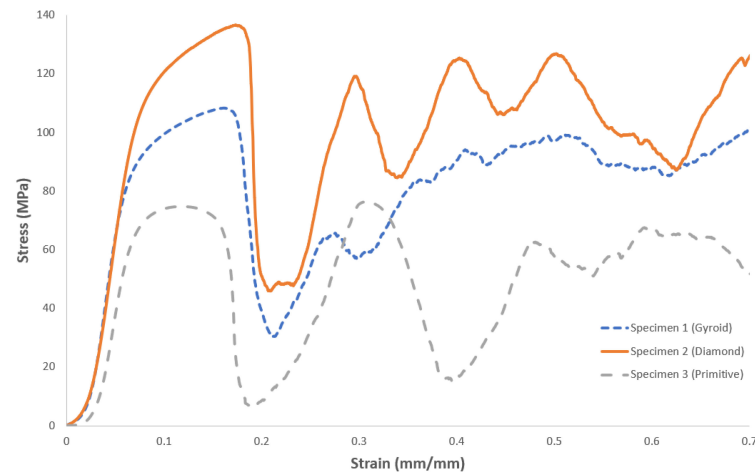

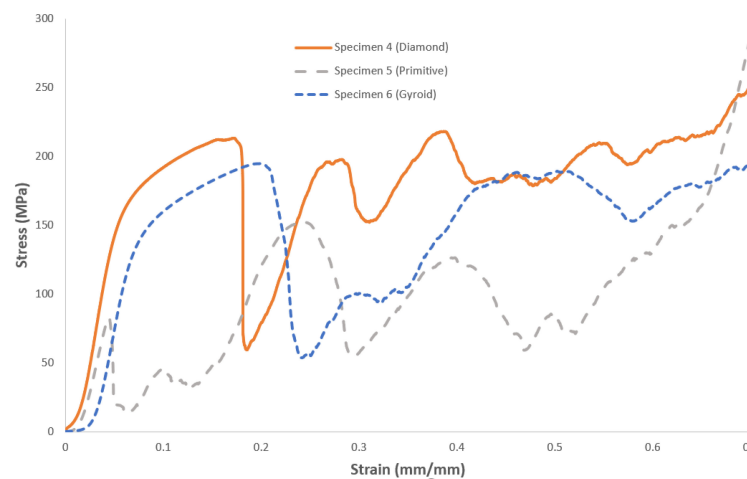**Figure 3.** Stress–strain graph for specimens with 0.2 volume fraction.

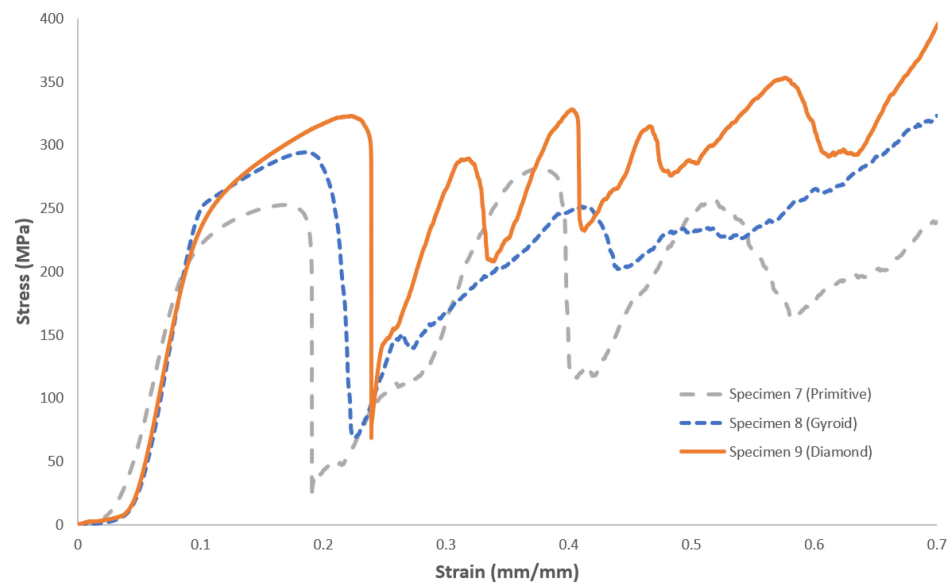**Figure 4.** Stress–strain graph for specimens with 0.3 volume fraction.

Figure 5. Stress–strain graph for specimens with 0.4 volume fraction.

In Figures 3–5, elastic, plastic, and densification regions can be clearly identified, where all specimens showed elastic behavior at low strains (0.1). For all specimens, the plastic collapse phenomena were observed at the onset of yield point.

It is well known that volume fraction has a great influence on the mechanical properties of lattice structures [36]. The Gibson–Ashby model is widely used to predict the compressive strength at various volume fractions or relative densities:

$$\frac{\sigma_{y_o}}{\sigma_y} = C \left(\frac{\rho_0}{\rho} \right)^{3/2} \tag{5}$$

where σ_{y_o} and ρ_o are the yield strength and density of full dense part, respectively. On the other hand, σ_y and ρ are the yield strength and density of lattice part, respectively. C is a scaling factor, ranging from 0.1 to 1 [37]. From Figures 3–5 and Table 4, it is clear that all specimens showed higher σ_y, E, and specific energy absorption at higher volume fractions, consistent with the Gibson–Ashby model. Zhang et al. [38] found similar results for stainless steel 316L Gyroid specimens produced by LPBF. They stated that all layers of the specimens collapsed simultaneously during compression and higher volume fractions resulted in higher σ_y, E, and specific energy absorption. Gyroid specimens showed a fluctuating plateau stress from 20–25% strain up to 70% strain, at which point, densification starts. In the plateau regime, several humps were observed. During compressive loading, struts or walls in the lattice structure collapse due to the cracks resulting in a drop of the stress. These struts or walls squeeze, resulting in an increase in stress up to the next fracture. This collapsing and squeezing of struts or walls is the main reason for the oscillating behavior of compressive stress–strain curves in lattice structures [39]. The difference between Gyroid specimens from Diamond and Primitive specimens is that Gyroid specimens have two layers in one unit cell, whereas Diamond and Primitive specimens have only one layer in one unit cell [19]. It is clear that with the increase of volume fractions, fluctuations in the plateau regime increase due to higher stiffness of the Gyroid specimens [15]. For Gyroid specimens, the onset stress of densification was 100 MPa for specimen 1, 190 Mpa for specimen 6, and 320 MPa for specimen 8, indicating that volume fraction increase has a great influence on the stress value at which densification begins. For Gyroid specimens, the deformation behavior in the densification stage was a rapid stress increase similar to those of solid parts [40]. At the end of the plateau regime and at the onset of the densification regime, specimens showed nearly full densification (resembling a solid, bulk part), meaning that much higher loading needs to be applied to get a small increase in strain.

Similar to the Gyroid specimens, Diamond specimens at higher volume fractions also continued to deform with more fluctuations beyond the elastic region when compared to the same specimens with lower volume fractions due to higher stiffness [15]. Diamond specimens (specimen 2, 4, and 9) showed a fluctuating plateau stress from 20–22% strain up to 60–70% strain, at which point, densification starts. The onset stress of densification for Diamond specimens was 125 MPa for specimen 2, 250 MPa for specimen 4, and 310 MPa for specimen 9. The trend with respect to volume fraction is similar to Gyroid specimens, meaning that volume fraction increase has a great influence on the stress value at which densification begins. Like Gyroid specimens, and also solid parts, the deformation behavior in the densification stage was a rapid stress increase.

Primitive specimens (specimen 3, 5, and 7) showed a fluctuating plateau stress from 5–15% strain up to 60–70% strain, at which point, densification starts. These specimens showed high fluctuations in the plateau regime compared to Gyroid and Diamond specimens. The onset stress of densification for Primitive specimens was 55 MPa for specimen 3, 130 MPa for specimen 5, and 240 MPa for specimen 7. Primitive specimens also showed a rapid stress increase behavior in densification stage, and the stress at the initiation of densification increased with increasing volume fraction.

3.2. ANOVA Results

3.2.1. ANOVA for σ_y

The main effect plot for σ_y is shown in Figure 6. It is clear that σ_y increases with an increase in volume fraction from 0.2 to 0.4 or with a decrease in build orientation from 90° to 45°. The optimal parameter set for σ_y was obtained at 0.4 volume fraction, and 45° build orientation with a Diamond structure. The worst parameter set related with σ_y was obtained at 0.2 volume fraction, and 90° build orientation with Primitive structure. During the compressive loading of lattice structures, cells collapse and walls of TPMS structures buckle. Higher volume fraction means less tendency for buckling due to less wall slenderness [4]. Therefore, higher σ_y was observed at higher volume fractions.
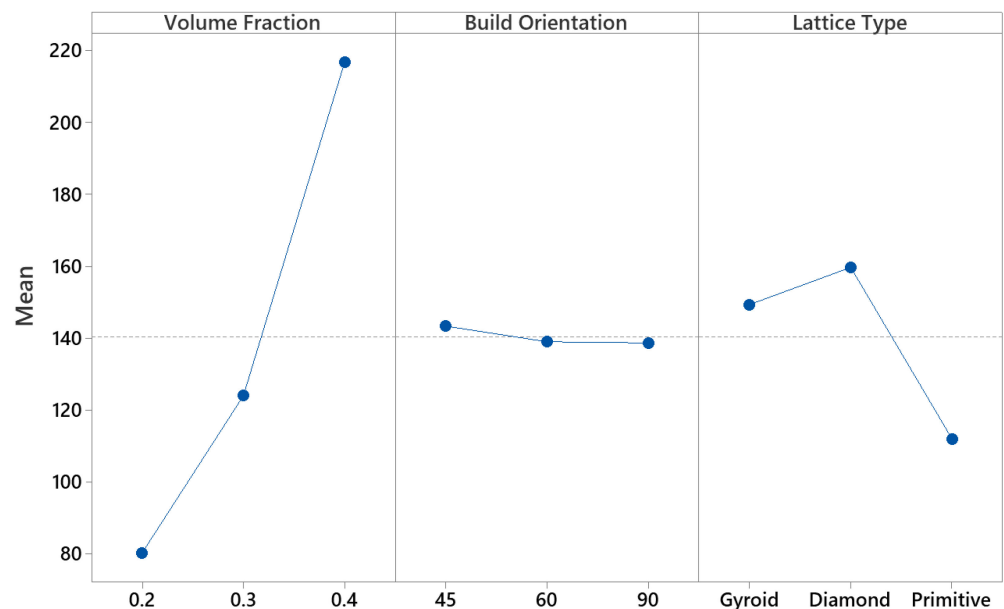

Figure 6. Main effect plot for σ_y.

The relative importance of the input parameters with respect to σ_y was investigated using ANOVA. ANOVA results for σ_y are shown in Table 5. In this table, DF stands for degree of freedom of the related parameter; Adj SS stands for adjusted sum of squares which are the measures of variations; Adj MS stands for adjusted mean squares, which measure how much variation the related parameter explains; F-value is used to calculate *p*-value,

which is used for evaluating the statistical significance of the related parameter. The percent contribution in Table 5 shows the relative importance of that parameter on the result (in this case, σ_y). According to the analysis, the most and the least effective input parameters with respect to σ_y are volume fraction and build orientation, respectively. The major factor affecting the σ_y is volume fraction, with a contribution of 85.11%, whereas lattice type was found to be the second ranking factor, with 11.04% contribution. The percent contribution of build orientation on σ_y was found to be insignificant (0.12%). Any change in build orientation resulted in a negligible change in the mean values, as represented in Figure 6. However, it is also clear from Figure 6 that a change in volume fraction resulted in a relatively much higher increase in mean values, consistent with Table 5.

Table 5. ANOVA results for σ_y.

Source	DF	Adj SS	Adj MS	F-Value	*p*-Value	Contribution
Volume Fraction	2	29,080.7	14,540.3	22.83	0.042	85.11%
Build Orientation	2	40.7	20.3	0.03	0.969	0.12%
Lattice Type	2	3772.7	1886.3	2.96	0.252	11.04%
Error	2	1274.0	637.0			3.73%
Total	8					100.00%

3.2.2. ANOVA for *E*

Main effect plot for *E* is shown in Figure 7. It is clear that *E* increases with an increase in volume fraction from 0.2 to 0.4. The optimal parameter set for *E* was obtained at 0.4 volume fraction, and 60° build orientation with a Gyroid structure. The worst parameter set related with *E* was obtained at 0.2 volume fraction, and 45° build orientation with a Primitive structure. The higher *E* values for Gyroid specimens when compared with Primitive specimens was also observed in [41].
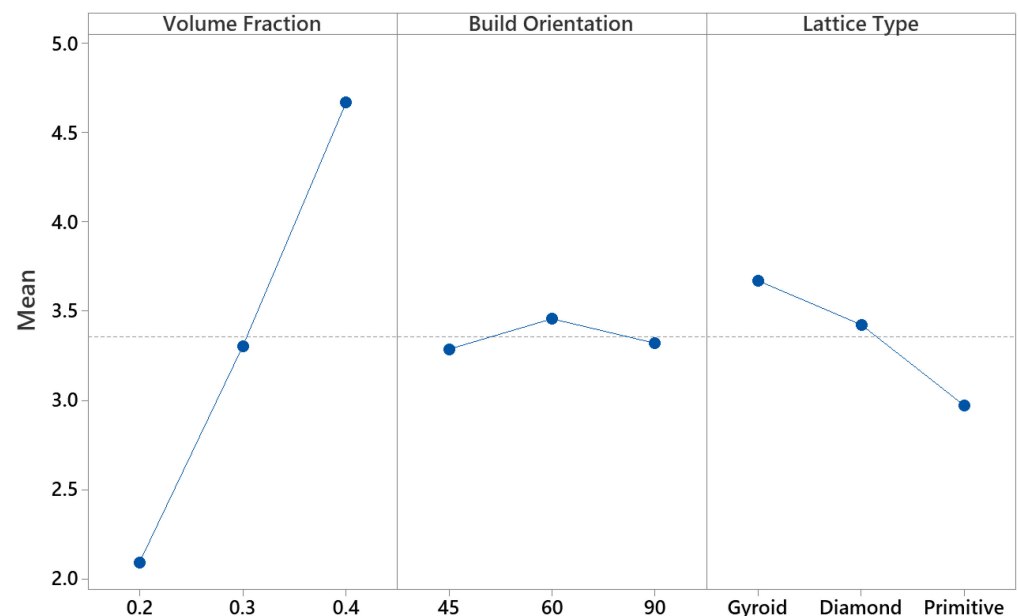

Figure 7. Main effect plot for *E*.

ANOVA results for *E* are shown in Table 6. According to the analysis, the most and the least effective input parameters with respect to *E* are volume fraction and build orientation, respectively. The major factor affecting the *E* is volume fraction, with a contribution of 91.83%, whereas lattice type was found to be the second ranking factor, with a 6.98% contribution. The percent contribution of build orientation on *E* was found to be insignificant (0.45%).
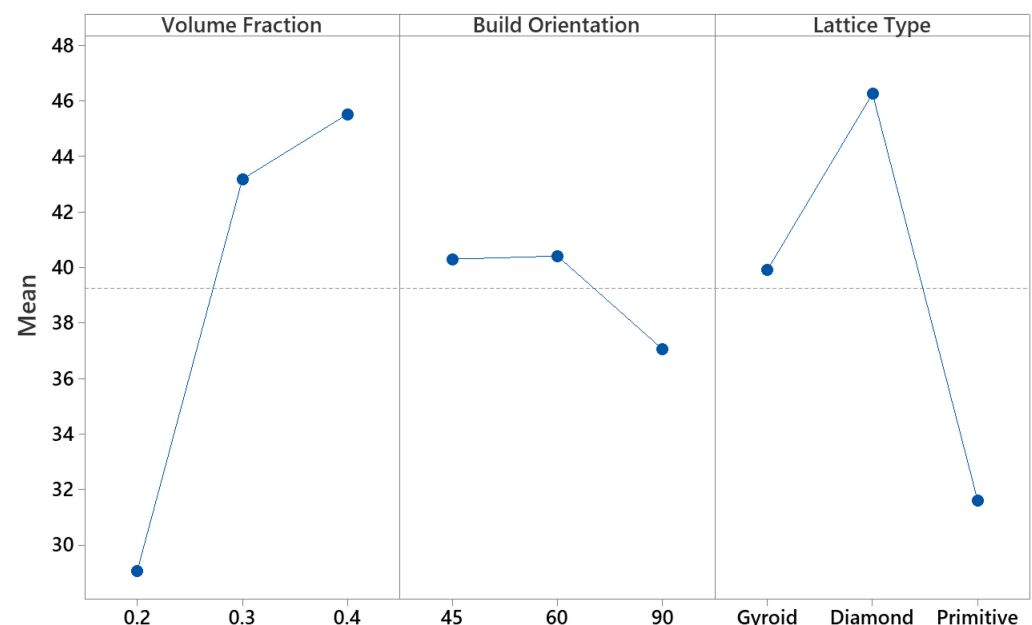
Table 6. ANOVA results for *E*.

Source	DF	Adj SS	Adj MS	F-Value	*p*-Value	Contribution
Volume Fraction	2	9.94482	4.97241	125.32	0.008	91.83%
Build Orientation	2	0.04869	0.02434	0.61	0.620	0.45%
Lattice Type	2	0.75636	0.37818	9.53	0.095	6.98%
Error	2	0.07936	0.03968			0.73%
Total	8					100.00%

Although the build orientation exhibited low relative importance on σ_y and *E*, it was also stated in some of the studies that strut/wall orientation (the orientation of struts in strut-based lattice structures, or the orientation of walls in TPMS-type lattice structures with respect to build or loading direction) changes with respect to build or loading direction, which results in a change in mechanical properties [42–44].

3.2.3. ANOVA for Specific Energy Absorption

The main effect plot for specific energy absorption is shown in Figure 8. Specific energy absorption increases with an increase in volume fraction from 0.2 to 0.4 or with a decrease in build orientation from 90° to 45°. The effect of volume fraction on specific energy absorption was also investigated by Zhang et al. [38], and a similar relation was observed. The optimal parameter set for specific energy absorption was obtained at 0.4 volume fraction, and 60° build orientation with a Diamond structure. The worst parameter set related with specific energy absorption was obtained at 0.2 volume fraction, and 90° build orientation with a Primitive structure. At higher volume fractions, Diamond specimens showed higher fluctuations or humps in the plateau regime than Gyroid and Primitive specimens, which increases the area under the stress–strain graph, and energy absorption behavior. Therefore, a Diamond structure is more feasible in energy absorption applications than Gyroid and Primitive structures. Novak et al.'s study [18] also showed that Diamond specimens outperformed Gyroid and Diamond specimens in terms of specific energy absorption.

Figure 8. Main effect plot for specific energy absorption.

ANOVA results for specific energy absorption are shown in Table 7. According to the analysis, the most and the least effective input parameters with respect to specific energy absorption are volume fraction and build orientation, respectively. The major factor affecting the specific energy absorption is volume fraction, with a contribution of 57.71%, whereas lattice type was found to be the second ranking factor, with 39.40%

contribution. The percent contribution of build orientation on specific energy absorption was found to be 2.63%.

Table 7. ANOVA results for specific energy absorption.

Source	DF	Adj SS	Adj MS	F-Value	*p*-Value	Contribution
Volume Fraction	2	474.152	237.076	221.11	0.005	57.71%
Build Orientation	2	21.647	10.823	10.09	0.090	2.63%
Lattice Type	2	323.695	161.848	150.95	0.007	39.40%
Error	2	2.144	1.072			0.26%
Total	8					100.00%

3.2.4. Multi Objective Optimization Based on Grey Relation Analysis

Since volume fraction, build orientation and lattice type have different effects on σ_y, E, and specific energy absorption, and since the optimal condition of these parameters for each of the performance outputs are different, as stated in Sections 3.2.1–3.2.3, a common single optimal condition for these three performance outputs needs to be evaluated by using multi objective optimization techniques. In this study, grey relation analysis was used, which is an efficient way of finding optimum process parameters involving multiple responses. The main effect plot for the three performance responses (σ_y, E, and specific energy absorption) is shown in Figure 9. It is clear that the Diamond specimen with 0.4 volume fraction and 45° build orientation outperformed in terms of three outputs. Primitive specimen with 0.2 volume fraction and 90° build orientation showed the worst results.
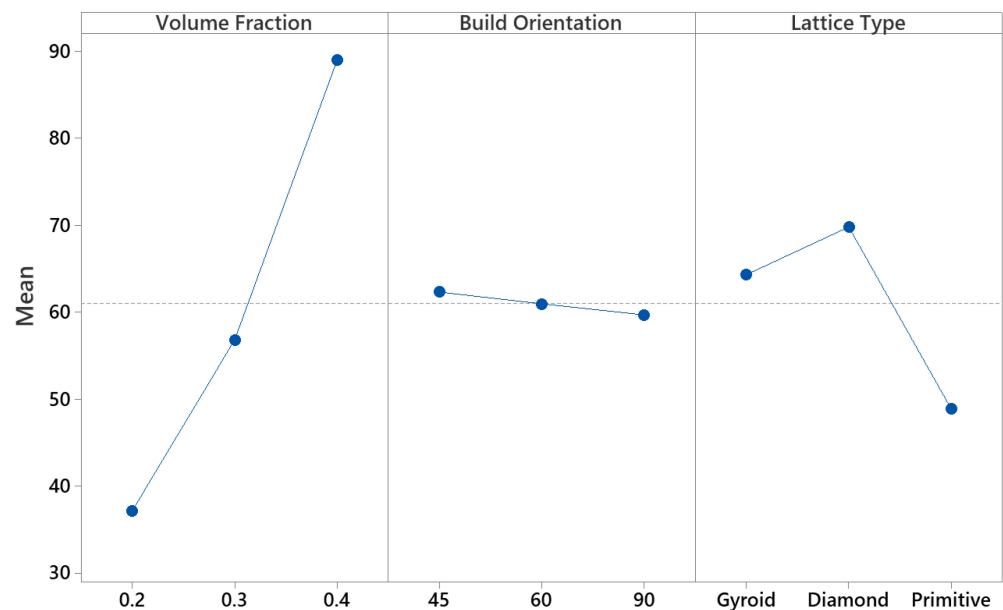

Figure 9. Main effect plot for multiple responses.

4. Conclusions

In this study, the effects of volume fraction, build orientation, and lattice type on compressive behavior of LPBF-manufactured CoCrMo specimens were investigated. Based on the experimental and statistical results, the following conclusions can be drawn:

1. Gyroid, Diamond, and Primitive specimens showed elastic behavior at low strains (10%). When exceeding yield point, a sudden plastic collapse was observed for all conditions.

2. Diamond specimens showed higher σ_y and specific energy absorption than Gyroid and Primitive specimens at the same volume fractions, except σ_y for 0.4 volume fraction, where the Gyroid specimen outperformed the Diamond specimen. For E values, Gyroid specimens outperformed Diamond and Primitive specimens for all volume fractions.

3. A volume fraction of 0.4, and 45° build orientation with a Diamond structure was found to be the best parameter set for σ_y. On the other hand, a 0.4 volume fraction, and 60° build orientation with Gyroid structure was the best parameter set for *E*. Finally, the Diamond structure with 0.4 volume fraction and 60° build orientation showed the highest specific energy absorption.

4. Multi objective optimization based on grey relation analysis showed that the Diamond specimen with 0.4 volume fraction and 45° build orientation was found to be the single optimum parameter set common for all three output parameters.

5. For all performance parameters (σ_y, *E*, and specific energy absorption), volume fraction and build orientation were found to be the major and minor affecting factors, respectively.

The scope of the study was constrained to three design parameters and three performance outputs. However, the following considerations can be taken into account as future studies:

- In the present study, 0.2, 0.3, and 0.4 volume fractions and 45, 60, and 90° build orientations were selected, and ANOVA analysis was based upon the mechanical performance results of these variables. A wider and intermediate range of volume fractions and build orientations can be used to better estimate the effect of these parameters on mechanical properties.

- The effect of dimensional variations, microstructure, and surface roughness on mechanical properties can also be evaluated.

- In the present study, only quasi-static compression tests were performed. The effect of design parameters on dynamic response of TPMS lattice structures can be investigated.

Author Contributions: Conceptualization, O.G. and U.S.; methodology, O.G.; validation, O.G., U.S. and M.Ö.; investigation, O.G.; resources, O.G.; data curation, G.G.Y. and O.C.; writing—original draft preparation, O.G.; writing—review and editing, U.S., G.G.Y. and P.Ş. All authors have read and agreed to the published version of the manuscript.

Institutional Review Board Statement: Not applicable.

Informed Consent Statement: Not applicable.

Data Availability Statement: The data presented in this study are available on request from the corresponding author.

Conflicts of Interest: The authors declare no conflict of interest. The funders had no role in the design of the study; in the collection, analyses, or interpretation of data; in the writing of the manuscript, or in the decision to publish the results.

References

1. Zhang, X.Z.; Leary, M.; Tang, H.P.; Song, T.; Qian, M. Selective electron beam manufactured Ti-6Al-4V lattice structures for orthopedic implant applications: Current status and outstanding challenges. *Curr. Opin. Solid State Mater. Sci.* **2018**, *22*, 75–99. [CrossRef]
2. Nakajima, H. Fabrication, properties and application of porous metals with directional pores. *Prog. Mater. Sci.* **2007**, *52*, 1091–1173. [CrossRef]
3. Dallago, M.; Winiarski, B.; Zanini, F.; Carmignato, S.; Benedetti, M. On the effect of geometrical imperfections and defects on the fatigue strength of cellular lattice structures additively manufactured via Selective Laser Melting. *Int. J. Fatigue* **2019**, *124*, 348–360. [CrossRef]
4. Maconachie, T.; Leary, M.; Lozanovski, B.; Zhang, X.; Qian, M.; Faruque, O.; Brandt, M. SLM lattice structures: Properties, performance, applications and challenges. *Mater. Des.* **2019**, *183*, 108–137. [CrossRef]
5. Lord, E.A.; Mackay, A.L. Periodic minimal surfaces of cubic symmetry. *Curr. Sci.* **2003**, *85*, 346–362.
6. Schoen, A.H. Infinite periodic minimal surfaces without self-intersections. In *NASA Technical Report TN D-5541*; NASA: Washington, DC, USA, 1970.
7. Koch, E.; Fischer, W. On 3-periodic minimal surfaces. *Z. Kristallogr.* **1987**, *179*, 31–52.

8. Gozdz, W.; Holyst, R. From the Plateau problem to periodic minimal surfaces in lipids and diblock copolymers. *Macromol. Theory Simul.* **1996**, *5*, 321–332.
9. Yadroitsev, I.; Yadroitsava, I.; Du Plessis, A. Basics of laser powder bed fusion. In *Additive Manufacturing Materials and Technologies, Fundamentals of Laser Powder Bed Fusion of Metals*, 1st ed.; Yadroitsev, I., Yadroitsava, I., du Plessis, A., MacDonald, E., Eds.; Elsevier: Holland, The Netherlands, 2021; pp. 15–38.
10. Deshpande, V.S.; Ashby, M.F.; Fleck, N.A. Foam topology bending versus stretching dominated architectures. *Acta Mater.* **2001**, *49*, 1035–1040. [CrossRef]
11. Maskery, I.; Sturm, L.; Aremu, A.O.; Panesar, A.; Williams, C.B.; Tuck, C.J.; Wildman, R.D.; Ashcroft, I.A.; Hague, R.J.M. Insights into the mechanical properties of several triply periodic minimal surface lattice structures made by polymer additive manufacturing. *Polymer* **2018**, *152*, 62–71. [CrossRef]
12. Restrepo, S.; Ocampo, S.; Ramirez, J.A.; Paucar, C.; Garcia, C. Mechanical properties of ceramic structures based on Triply Periodic Minimal Surface (TPMS) processed by 3D printing. *J. Phys. Conf. Ser.* **2017**, *935*, 012036. [CrossRef]
13. Castro, A.P.G.; Santos, J.; Pires, T.; Fernandes, P.R. Micromechanical behavior of tpms scaffolds for bone tissue engineering. *Macromol. Mater. Eng.* **2020**, *305*, 2000487. [CrossRef]
14. Abueidda, D.W.; Elhebeary, M.; Shiang, C.-S.; Pang, S.; Abu Al-Rub, R.K.; Jasiuk, I.M. Mechanical properties of 3D printed polymeric Gyroid cellular structures: Experimental and finite element study. *Mater. Des.* **2019**, *165*, 107597. [CrossRef]
15. Al Mahri, S.; Santiago, R.; Lee, D.W.; Ramos, H.; Alabdouli, H.; Alteneiji, M.; Guan, Z.; Cantwell, W.; Alves, M. Evaluation of the dynamic response of triply periodic minimal surfaces subjected to high strain-rate compression. *Addit. Manuf.* **2021**, *46*, 102220.
16. Zhang, L.; Feih, S.; Daynes, S.; Chang, S.; Wang, M.Y.; Wei, J.; Lu, W.F. Energy absorption characteristics of metallic triply periodic minimal surface sheet structures under compressive loading. *Addit. Manuf.* **2018**, *23*, 505–515. [CrossRef]
17. Liang, Y.; Zhou, W.; Liu, Y.; Li, Z.; Yang, Y.; Xi, H.; Wu, Z. Energy absorption and deformation behavior of 3d printed triply periodic minimal surface stainless steel cellular structures under compression. *Steel Res. Int.* **2021**, *92*, 2000411. [CrossRef]
18. Novak, N.; Al-Ketan, O.; Krstulović-Opara, L.; Rowshan, R.; Abu Al-Rub, R.K.; Vesenjak, M.; Ren, Z. Quasi-static and dynamic compressive behaviour of sheet TPMS cellular structures. *Compos. Struct.* **2021**, *266*, 113801. [CrossRef]
19. Shi, X.; Liao, W.; Li, P.; Zhang, C.; Liu, T.; Wang, C.; Wu, J. Comparison of compression performance and energy absorption of lattice structures fabricated by selective laser melting. *Adv. Eng. Mater.* **2020**, *22*, 2000453. [CrossRef]
20. Rashed, M.G.; Ashraf, M.; Mines, R.A.W.; Hazell, P.J. Metallic microlattice materials: A current state of the art on manufacturing, mechanical properties and applications. *Mater. Des.* **2016**, *95*, 518–533. [CrossRef]
21. Cai, Z.; Liu, Z.; Hu, X.; Kuang, H.; Zhai, J. The effect of porosity on the mechanical properties of 3D-printed triply periodic minimal surface (TPMS) bioscaffold. *Bio-Des. Manuf.* **2019**, *2*, 242–255. [CrossRef]
22. Alsalla, H.; Hao, L.; Smith, C. Fracture toughness and tensile strength of 316L stainless steel cellular lattice structures manufactured using the selective laser melting technique. *Mater. Sci. Eng. A* **2016**, *669*, 1–6. [CrossRef]
23. Delroisse, P.; Jacques, P.J.; Maire, E.; Rigo, O.; Simar, A. Effect of strut orientation on the microstructure heterogeneities in AlSi10Mg lattices processed by selective laser melting. *Scr. Mater.* **2017**, *141*, 32–35. [CrossRef]
24. Brodie, E.G.; Wegener, T.; Richter, J.; Medvedev, A.; Niendorf, T.; Molotnikov, A. A mechanical comparison of alpha and beta phase biomedical TiTa lattice structures. *Mater. Des.* **2021**, *212*, 110220. [CrossRef]
25. Seede, R.; Mostafa, A.; Brailovski, V.; Jahazi, M.; Medraj, M. Microstructural and microhardness evolution from homogenization and hot isostatic pressing on selective laser melted Inconel 718: Structure, texture, and phases. *J. Manuf. Mater. Process.* **2018**, *2*, 30. [CrossRef]
26. Zhang, B.; Wang, P.; Chew, Y.; Wen, Y.; Zhang, M.; Wang, P.; Bi, G.; Wei, J. Mechanical properties and microstructure evolution of selective laser melting Inconel 718 along building direction and sectional dimension. *Mater. Sci. Eng. A* **2020**, *794*, 139941. [CrossRef]
27. Britt, C.; Montgomery, C.J.; Brand, M.J.; Liu, Z.K.; Carpenter, J.S.; Beese, A.M. Effect of processing parameters and strut dimensions on the microstructures and hardness of stainless steel 316L lattice-emulating structures made by powder bed fusion. *Addit. Manuf.* **2021**, *40*, 101943. [CrossRef]
28. Qi, M.; Huang, S.; Ma, Y.; Youssef, S.S.; Zhang, R.; Qiu, J.; Lei, J.; Yang, R. Columnar to equiaxed transition during β heat treatment in a near β alloy by laser additive manufacture. *J. Mater. Res. Technol.* **2021**, *13*, 1159–1168. [CrossRef]
29. Ravichander, B.B. Correlation and Effect of Process Parameters on the Properties of Inconel 718 Parts Fabricated by Selective Laser Melting Using Response Surface Method. Master's Thesis, The University of Texas at Arlington, Arlington, TX, USA, 2020.
30. Dong, G.; Wijaya, G.; Tang, Y.; Zhao, Y.F. Optimizing process parameters of fused deposition modeling by Taguchi method for the fabrication of lattice structures. *Addit. Manuf.* **2018**, *19*, 62–72. [CrossRef]
31. Park, S.-Y.; Kim, K.-S.; AlMangour, B.; Grzesiak, D.; Lee, K.-A. Compressive deformation behavior and energy absorption characteristic of additively manufactured sheet CoCrMo triply periodic minimal surface lattices. *J. Mater. Res. Technol.* **2022**, *18*, 171–184. [CrossRef]
32. Box, G. Signal-to-noise ratios, performance criteria, and transformations. *Technometrics* **1988**, *30*, 1–17. [CrossRef]
33. Pan, C.; Han, Y.; Lu, J. Design and optimization of lattice structures: A review. *Appl. Sci.* **2020**, *10*, 6374. [CrossRef]
34. Tan, X.; Wang, P.; Kok, Y.; Toh, W.; Sun, Z.; Nai, S.; Descoins, M.; Mangelinck, D.; Liu, E.; Tor, S.B. Carbide precipitation characteristics in additive manufacturing of Co-Cr-Mo alloy via selective electron beam melting. *Scr. Mater.* **2017**, *143*, 117–121. [CrossRef]

35. Ozeren, E.; Altan, M. Effect of structural hybrid design on mechanical and biological properties of CoCr scaffolds fabricated by selective laser melting. *Rapid Prototyp. J.* **2019**, *26*, 615–624. [CrossRef]
36. Yan, C.; Hao, L.; Hussein, A.; Young, P.; Huang, J.; Zhu, W. Microstructure and mechanical properties of aluminium alloy cellular lattice structures manufactured by direct metal laser sintering. *Mater. Sci. Eng. A* **2015**, *628*, 238–246. [CrossRef]
37. Ashby, M.F. The properties of foams and lattices. *Philos. Trans. R. Soc. A* **2006**, *364*, 15–30. [CrossRef] [PubMed]
38. Zhang, C.; Zheng, H.; Yang, L.; Li, Y.; Jin, J.; Cao, W.; Yan, C.; Shi, Y. Mechanical responses of sheet-based gyroid-type triply periodic minimal surface lattice structures fabricated using selective laser melting. *Mater. Des.* **2022**, *214*, 110407. [CrossRef]
39. Yan, C.; Hao, L.; Hussein, A.; Bubb, S.L.; Young, P.; Raymont, D. Evaluation of light-weight AlSi10Mg periodic cellular lattice structures fabricated via direct metal laser sintering. *J. Mater. Process. Technol.* **2014**, *4*, 856–864. [CrossRef]
40. Yu, S.; Sun, J.; Bai, J. Investigation of functionally graded TPMS structures fabricated by additive manufacturing. *Mater. Des.* **2019**, *182*, 108021. [CrossRef]
41. Abueidda, D.W.; Abu Al-Rub, R.K.; Dalaq, A.S.; Lee, D.; Khan, K.A.; Jasiuk, I. Effective conductivities and elastic moduli of novel foams with triply periodic minimal surfaces. *Mech. Mater.* **2016**, *95*, 102–115. [CrossRef]
42. Cansizoglu, O.; Harrysson, O.; Cormier, D.; West, H.; Mahale, T. Properties of Ti–6Al–4V non-stochastic lattice structures fabricated via electron beam melting. *Mater. Sci. Eng. A* **2008**, *492*, 468–474. [CrossRef]
43. McKown, S.; Shen, Y.; Brookes, W.K.; Sutcliffe, C.J.; Cantwell, W.J.; Langdon, G.S.; Nurick, G.N.; Theobald, M.D. The quasi-static and blast loading response of lattice structures. *Int. J. Impact Eng.* **2008**, *35*, 795–810. [CrossRef]
44. Yan, C.; Hao, L.; Hussein, A.; Young, P.; Raymont, D. Advanced lightweight 316L stainless steel cellular lattice structures fabricated via selective laser melting. *Mater. Des.* **2014**, *55*, 533–541. [CrossRef]